



Fluid targeted delivery of functionalized magnetoresponsive nanocomposite particles to a ferromagnetic stent

Sandor I. Bernad^{a,*}, Izabell Craciunescu^b, Gurpreet S. Sandhu^c, Dan Dragomir-Daescu^{d,*},
Etelka Tombacz^e, Ladislau Vekas^a, Rodica Turcu^{b,*}

^a Centre for Fundamental and Advanced Technical Research, Romanian Academy, Timisoara Branch, 300223 Timisoara, Romania

^b National Institute for Research and Development of Isotopic and Molecular Technologies, Donat Str. 67-103, 400293 Cluj-Napoca, Romania

^c Department of Cardiovascular Medicine, Mayo Clinic, 200 First St SW, Rochester, MN 55905, USA

^d Department of Physiology and Biomedical Engineering, Mayo Clinic, 200 First St SW, Rochester, MN 55905, USA

^e Department of Food Engineering, University of Szeged, Moszkvai krt. 5-7, H-6725 Szeged, Hungary

ARTICLE INFO

Keywords:

Magnetic particle targeting
PEG coating
Ferromagnetic stent
Biocompatibility
Hemodynamics

ABSTRACT

Vascular stent implantation needs a rapid endothelialization to reduce morbidity and improve patient outcomes. A promising strategy to enhance the artery wall healing is to use the site-specific drug targeting technique to deliver the required medication at the site of injury. This work presents a new concept of using permanent magnet systems to guide and target the functionalized magnetoresponsive nanocomposite clusters around the ferromagnetic stent. In our experiment, the PEG-coated magnetic clusters capture and deposition are based on the competition between the drag force and the magnetic force exerted by both the magnetic field gradient generated by the permanent external magnet and the ferromagnetic stent. Also, the ferromagnetic stent was tested for biological toxicity, and the result shown the excellent device biocompatibility. Stent magnetic particle targeting process generates an almost uniform strut coverage with PEG-coated MNP's within the different stent segments (proximal, central, and distal segment), but visibly different between stent segments. The magnetic clusters deposition stability in time demonstrates that stent struts coverage remains quasi constant after 1 min of exposure to the flow shear stress.

1. Introduction

Implantation of a rigid stent in the arterial system imposes alterations to the arterial geometry and creates focal geometric irregularities due to the strut protrusion [1]. Stent deployment alters the geometric flow boundary conditions due to the protrusion of stent struts into the flow stream, resulting in hemodynamic parameters changing local blood flow patterns [2]. The presence of the stent causes acute artery response like neointimal hyperplasia (NH) and in-stent restenosis (ISR), developed after stent insertion [3]. Vascular wall deformations modify flow velocity profiles, reduce the endothelial shear stress (ESS) along the length of the stented arterial segment, and alter the focal in-stent ESS distribution [4].

Vascular injury leads to the activation of various biological cells and the release of numerous vasoactive, thrombogenic, and mitogenic factors in the restenosis process [5].

To reduce these disadvantages of the first-generation bare-metal

stents (BMS), drug-eluting stents (DES) are currently widely used in clinical practice. The time course of the vascular healing process after DES placement varies from patient to patient; consequently, all patients with high risk for late thrombosis should receive dual antiplatelet therapy for prolonged periods [6,7].

Several clinical trials present different recommendations for the duration of dual antiplatelet therapy. For example, two European trials recommend less than six months of antiplatelet treatment [8,9]; instead, there is a larger FDA-sponsored US trial recommend at least 30 months antiplatelet therapy [10].

An effective strategy for counterbalance these shortcomings and improve the vascular wall healing performance after stent placement is to use the site-specific drug targeting technique to deliver the required medication using a minimally invasive procedure [11].

Among the magnetic carriers for medical use, magnetic iron oxide nanoparticles and their nanocomposites engineered with a large variety of functional coatings are the most promising [12-14]. The design of the

* Corresponding authors.

E-mail addresses: sandor.bernad@upt.ro (S.I. Bernad), dragomirdaescu.dan@mayo.edu (D. Dragomir-Daescu), rodica.turcu14@gmail.com (R. Turcu).

<https://doi.org/10.1016/j.jmmm.2020.167489>

Received 3 July 2020; Received in revised form 29 September 2020; Accepted 9 October 2020

Available online 22 October 2020

0304-8853/© 2020 Elsevier B.V. All rights reserved.

organic coating and its grafting at the magnetic nanoparticle (MNPs) surface is a crucial challenge. The nature of MNP's surface coating should ensure biocompatibility and stability, preventing the nonspecific adhesion of plasma proteins on the surface of MNPs.

From diagnosis and treatment point of view, due to the magnetic response in targeting or MRI detection, the iron oxide nanoparticle assemblies receiving continuously increasing interest [15]. For example, successful biomedical applications, particularly magnetic drug targeting, explore the advantages of the high magnetic moment of the functionalized multi-core carriers [16].

It is known that multi-core particles have no permanent magnetic moment, but the resultant magnetic moment of multi-core particles is parallel to the external magnetic field. Biomedical applications of magnetic nanoparticles and nanocomposites explore these abilities to be manipulated using magnetic fields [17].

In current practices, the most preferred approach to coat the magnetic iron oxide nanoparticles (IONPs) is to use hydrophilic polymers to bond the surface of the nanoparticles chemically using several coating agents (polyethylene oxides or glycols - PEG and polysaccharides like dextran [18]).

PEGylation reduces the non-specific adsorption of blood proteins generating a biologically passive surface around the MNPs, protecting particles from adhesion of inflammatory cells of phagocytes [19]. Results presented in the literature [20] proved that in the case of PEG-coated nanoparticles, the interaction with other biomolecules and proteins is influenced by the charge and hydrophobic/hydrophilic property of the surface of nanoparticles.

From the biomedical applications' point of view, PEG-coated MNPs must not be identified by the recognition system as foreign bodies. However, proteins can bind to PEG coatings and most likely retain their natural conformation [21,22].

Our previous publication [23] describes the synthesis of PEG-coated magnetite nanoparticles, the colloidal and magnetic properties of the core-shell, and their biocompatibility and potential for biomedical application.

Biocompatibility of the PEG-coated MNPs was evaluated using various selected tests, including hemocompatibility (interaction with human blood) investigated in the erythrocyte sedimentation rate (ESR) [22-24]. All the obtained ESR values agreed within the margin of error (± 3 mm/h) [23]. The PEGylated nanoparticles did not affect the rate of erythrocyte sedimentation, meaning that the human blood's colloidal state remained unchanged. Blood sedimentation experiments were performed to test the biocompatibility of PEGylated nanomagnets through their erythrocyte cytotoxicity. We also tested the change in the shape of the red blood cells; the results showed that the addition of the PEGylated nanoparticles does not induce the thrombocyte aggregation [25].

In our early reports [26], we have validated the ability to magnetically capture living endothelial cells on stents or vascular grafts [27]. The challenge regarding this technique is regarded as the used magnetic stent because the commercial stent was non-magnetizable. Also, the most magnetizable metals candidate for stent production were non-biocompatible or lacked the mechanical properties require for stent [28].

Taking into account the medical requirements imposed on a stent, respectively the need to be able to magnetically functionalized for the capture of the appropriately labeled nanoparticles, we recently developed a novel duplex stainless steel bare metal stent that can be used for nanotechnology-based applications [29], in particular for magnetic targeting.

The purpose of the current study was to develop a new concept of using permanent magnet systems to guide and target the functionalized magnetoresponsive nanocomposite particles around the ferromagnetic stent in the relevant hemodynamic milieu to test the ability to treat coronary heart disease (CHD).

The basic concept is to use the permanent magnet to provide an

enough strong magnetic field to guide and deposit the magnetoresponsive nanocomposite particles inside the implanted stent.

The novelty of this article, compared to the previously published results, consists of the following aspects:

- as carrier particle the PEG-coated magnetoresponsive nanocomposite particles were used compared to the PLGA poly(lactic-glycolic acid) coated magnetite used in previous work [26];
- in the present work the PEG-coated magnetic clusters with sizes in the range 40–150 nm (suitable for biomedical applications, in particular for particle targeting) were used against the 60 nm size PLGA coated SPION [30], or 6 to 10 μ m size iron particles [31,32] investigated in our previous work;
- the targeted device used a magnetically functionalized ferromagnetic stent. It was fashioned in correspondence with clinically used stent dimensions, namely 3.15×15 mm (Diameter \times Length) placed in the realistic artery model fashioned from acrylic glass;
- a Neodymium type external permanent magnet was used to generate the required constant magnetic field.

2. Experimental setup

2.1. Synthesis and characterization of magnetic clusters coated with PEG

2.1.1. Synthesis of magnetic clusters coated with PEG

Ferrofluid containing oleic acid (OA) monolayer-coated magnetite nanoparticles stably dispersed in toluene, prepared according to the procedure of Bica [33], was obtained from the Lab. Magnetic Fluids from Timisoara. Polyethylene glycol (PEG) were purchased from Sigma-Aldrich and used as received.

The PEG-coated magnetic clusters (PEG_CMC) were prepared using the oil-in-water miniemulsion method [34]. Toluene based ferrofluid (0.5 wt% Fe₃O₄) was added to an aqueous solution containing PEG (1.795 g), which acts as a surfactant. The presence of PEG molecules resulted in the formation of micelles, where PEG molecules organized themselves with the polar end in the water phase and the nonpolar end in the oil phase. The as created droplets contained the magnetic nanoparticles dispersed in toluene. To obtain a stable miniemulsion, the two-phase mixture was homogenized using an ultrasonic finger U.P. 400S, for 2 min. In the second step, the organic phase, toluene, was evaporated under magnetic stirring (500 rpm), at 100°C in an oil bath. The as-prepared magnetic clusters were subsequently washed with the methanol-water mixture (50 ml) to remove any excess of reactants and then redispersed in distilled water.

2.1.2. Characterization of the PEG coated magnetic clusters (PEG_CMC)

The morphology of the magnetic clusters was investigated by electron microscopy (STEM) on a Hitachi HD2700.

The surface chemical composition of magnetic clusters was investigated by X-ray Photoelectron Spectroscopy (XPS) using an XPS spectrometer SPECS equipped with a dual-anode X-ray source Al/Mg, a PHOIBOS 150 2D CCD hemispherical energy analyzer and a multi-channeltron detector with vacuum maintained at 1×10^{-9} torr. The AlK α X-ray source (1486.6 eV) operated at 200 W was used for XPS investigations. The particle suspension was dried on an indium foil to allow the XPS measurements. Data analysis and curve fitting were performed using CasaXPS software with a Gaussian-Lorentzian product function and a non-linear Shirley background subtraction.

The static magnetization of the samples was measured at room temperature by using a Vibrating Sample Magnetometer Cryogenics.

The representative TEM images of the PEG_CMC are shown in Fig. 1. Magnetite nanoparticles from the ferrofluid are packed into spherical clusters with sizes in the range 40–150 nm.

XPS analysis was used to demonstrate the successful coating of the magnetic clusters with PEG. Fig. 2 shows the XPS high-resolution spectra of C 1s, O 1s, and Fe 2p core-levels from PEG_CMC. The deconvolution of

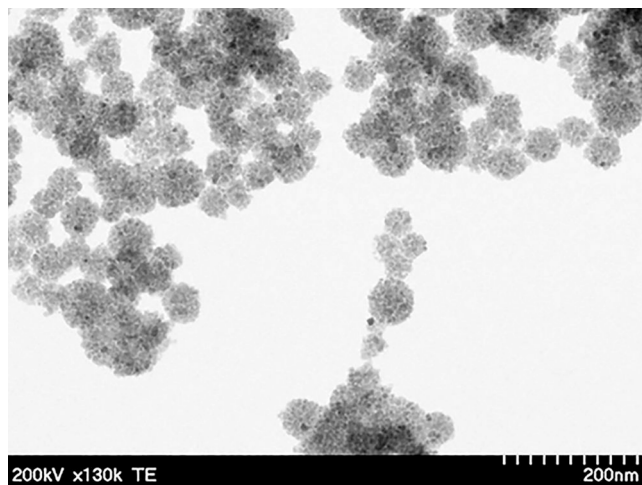


Fig. 1. TEM image of the magnetic clusters coated with PEG.

C 1s and O 1s spectra shows the contributions from the peaks assigned to specific groups of the nanoparticle's surfactant oleic acid and PEG coating of the clusters. The best fit of the C 1s spectrum was obtained with three components corresponding to C-C, C-H (284.7 eV); C-O (286.6 eV); O-C=O (288.9 eV). The O 1s spectrum exhibits three elements ascribed to Fe-O (530.2 eV), C-O (531.8 eV), O-C=O (533 eV). The Fe 2p spectrum contains the doublet Fe 2p_{3/2} and Fe 2p_{1/2}.

The magnetization curve of PEG_CMC at room temperature presented in Fig. 3 evidence a super-paramagnetic behavior. This fact demonstrates that the magnetite nanoparticles coated with oleic acid from the ferrofluid having mean sizes less than 10 nm are still well separated after cluster formation. The saturation magnetization of the PEG_CMC has a relatively high value of 56 emu/g.

2.2. Blood analog fluid preparation

As described in our previous study [32], for working fluid was used a blood analog fluid, which has the density (ρ) the same to the blood density (1060 kg/m³). In the present study, the flow was steady and contain minimal regions with shear rates lower than 10 sec⁻¹ (in the close vicinity of the bent segment of the stent), the blood viscosity model does not include viscoelasticity [32].

2.2.1. Rheological properties of the blood analog fluid

For blood, analog was used as carrier fluid (CF) prepared from glycerol-water solutions by mixing calculated weights of distilled water and glycerol. Viscosity curves at T = 25 °C of carrier fluid presented in Fig. 4 indicates a shear-thinning behavior at low shear rates, which becomes Newtonian at shear rates > 10 s⁻¹.

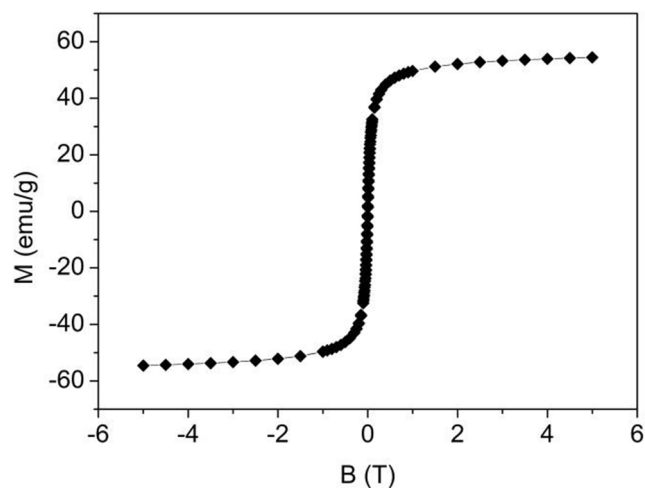


Fig. 3. Magnetization curve at room temperature of the PEG_CMC.

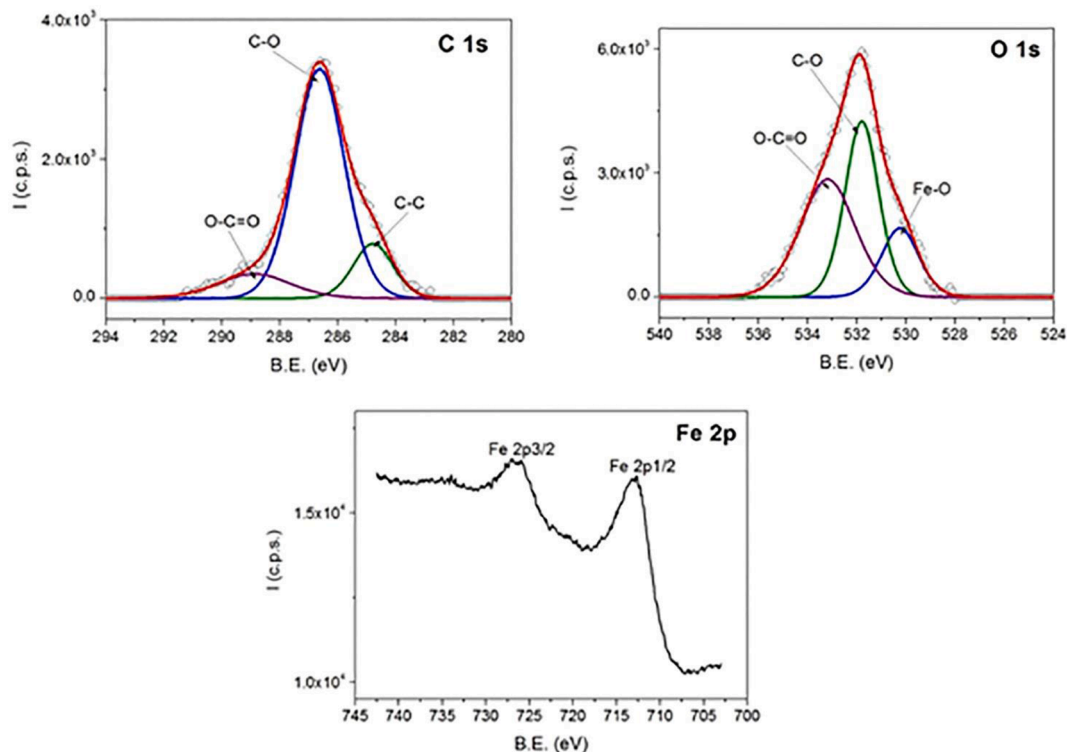


Fig. 2. High-resolution XPS spectra of C 1s (left), O 1s (right) and Fe 2p (bottom) core levels from magnetic clusters coated with PEG.

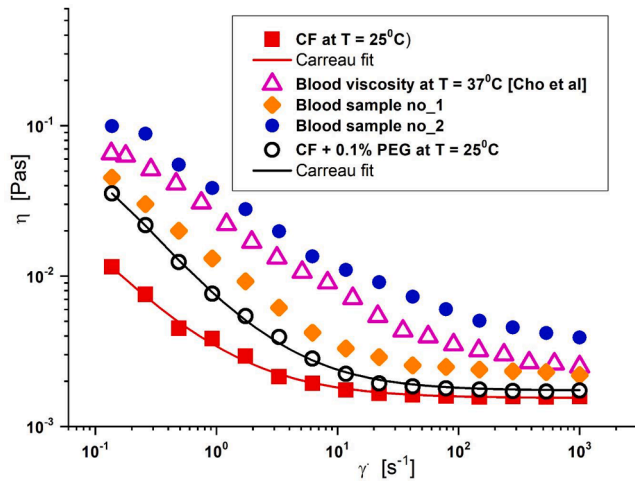


Fig. 4. Comparison between the viscosity curves of the carrier fluid (CF), the used model suspension fluid (CF + 0.1% PEG-coated magnetic clusters) and blood, for different working temperatures.

In this paper, the stent particle targeting performances were investigated using the functionalized magnetoresponsive nanocomposite particles. The model suspension of magnetic carriers used in experiments was obtained, mixing blood analog carrier fluid (CF) with the PEG_CMC dispersed in distilled water, with 0.1% mass concentration. Magneto-viscous characteristics were measured using a rotational rheometer (MCR 300, Physica, Stuttgart, Germany). It is important to note in Fig. 4 that the model suspension (CF + 0.1% PEG) viscosity curve was very similar to that of blood sample no.1, obtained from a healthy volunteer (female, age 38). The model suspension viscosity curve was also in good agreement with the viscosity curve of blood sample no.2 (healthy volunteer, female, age 49) and with results obtained by Cho et al. [35].

The degree of change in the model suspension depends on the generated magnitude of the applied field. As can be seen in Fig. 5, the MNP's used as model suspensions exhibited the required responsiveness

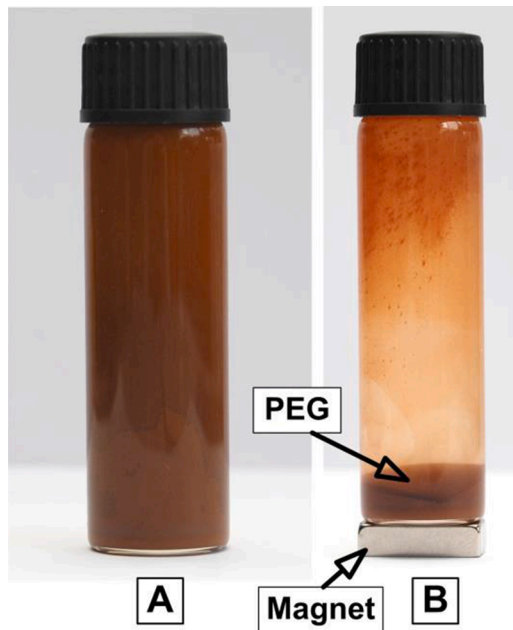


Fig. 5. PEG_CMC separation in the presence of the magnetic field. A) Prepared, PEG_CMC suspension. B) MNP's separation in the presence of the magnetic field.

to the action of a magnetic field. Placing a magnet in the vicinity of the bottle, the magnetic clusters are attracted by the permanent magnet (Fig. 5C and 5D), while in the absence of the magnetic field, the coated MNP's can readily disperse in the suspensions (Fig. 5A).

Fig. 4 shows that the model suspension (PEG_CMC dispersed in water-glycerol carrier) also exhibit shear-thinning behavior in the absence of the magnetic field, probably due to the shear-thinning character of the carrier fluid, and to the small aggregates of the magnetic cluster, that are progressively destroyed with shear intensification. The rheological values for both the CF and the model suspensions are presented in Table 1 and can be described using the Carreau model with four relevant parameters Eq. (1) [36,37].

$$\eta(\dot{\gamma}) = \eta_{\infty} + (\eta_0 - \eta_{\infty}) [1 + (C\dot{\gamma})^2]^{-p} \quad (1)$$

where η_0 is zero shear viscosity, η_{∞} is the viscosity at infinite shear rates, C is the characteristic time constant, and p is the flow behavior index. The fit parameters obtained to fit the experimental data are presented in Table 1.

- The R^2 values for all fits are close to the unity, indicating an excellent fit (R^2 – is the coefficient of determination used to evaluate the quality of the Carreau fits).

It is essential to mention that the wall shear stress (WSS) was practically derived from the friction of the flowing blood on the endothelial surface of the arterial wall. In the present paper, the particle targeting possibilities for a stented artery was investigated for the WSS value in a pathology [interval of 5 s^{-1} to 1000 s^{-1}] and normal range [interval of 0.1 s^{-1} to 5 s^{-1}] corresponding to the blood flow in the stented artery delivered after the coronary percutaneous intervention [38] (Fig. 4).

2.3. Experimental setup

The experimental setup used for the particle targeting of the stented artery is shown in Fig. 6 (the general concept of this setup was described in detail in our previous work [31,32]).

PEG_CMC suspensions were injected into the main flow (generated by the computer-controlled pump - GAMPT, Germany – centrifugal multi-flow pump) upstream of the artery model inlet section. The microliter syringe pump pushes the carrier fluid into the main flow. Injecting the PEG_CMC suspension at a distance of $19D_{st}$ (D_{st} – magnetic stent diameter) before the stent inlet section, facilitated dispersion of the nanoparticles in the fluid flow stream at the entrance of the artery model.

The following measurements procedure was used for targeting investigation:

1. The main flow was adjusted up to 0.25 m/s , corresponding to the 117 ml/min flow rate [39].
2. The permanent magnet was positioned to the desired distance from the bottom wall (15 mm) of the artery model region, and 18.15 mm from the upper part of the implanted stent.
3. The PEG_CMC suspension injection into the main flow was done for two interval times, namely, for 30 and 70 s , both at one minute after

Table 1

Rheological characterization of the carrier fluid and PEG particle suspensions.

Fluid	t [°C]	B [mT]	η_{∞} [Pas]	η_0 [Pas]	C [s]	p [–]	R^2
CF – carrier fluid	25	0	0.0015	0.193	244.48	0.421	0.997
CF + 0.1% PEG	25	0	0.00207	0.0749	15.757	0.475	0.9985

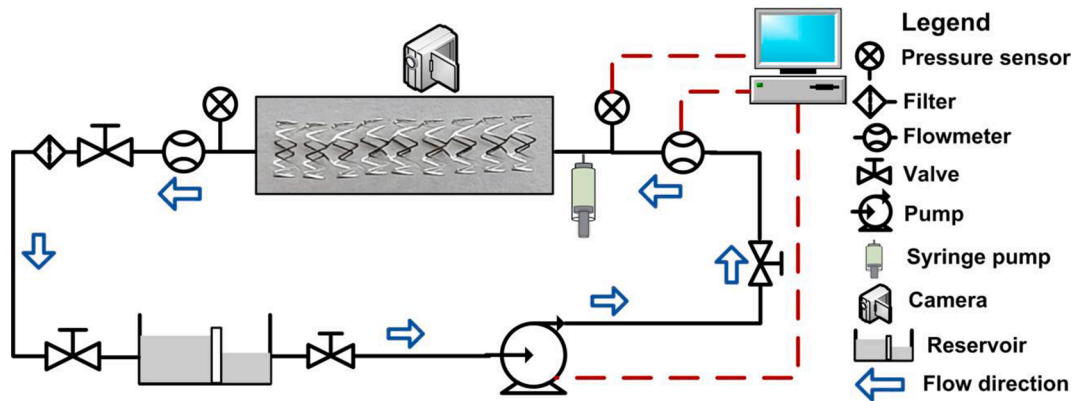


Fig. 6. The experimental setup used for magnetic stent investigations. The block diagram of the main recirculating flow loop contained: flowmeter, suspension injection mechanism – syringe pump, test section – magnetic stent model, valve, particle filter, reservoir, centrifugal pump. Syringe pump injects suspension in front of the magnetic stent model entry section.

the carrier flow start. During this time interval, the particle deposition around the magnetic stent we investigated using an image analysis technique.

4. A 20 ml syringe was used to inject a sample of the model suspension (PEG_CMC + carrier fluid) in front of the implanted stent at the desired constant flow rate using a syringe pump (a variable-speed infusion pump, GAMPT, Germany).
5. The model's suspension injection was performed at a constant flow rate of 39.6 ml/min for the 30 s injection time and 17.16 ml/min for the 70 s injection period.
6. PEG_CMC clusters mean diameter is around 85 nm, size range 40 to 150 nm.

Flow field and the nanoparticle distribution in the site of the stented artery region were investigated using the image analysis technique (CCD camera record, both flow dynamics and particle depositions in the area of interest).

2.3.1. Magnetic stent model

Commercially available stents can be classified according to their material (stainless steel, nitinol, cobalt-based alloy, tantalum, or biodegradable) their design (ring, mesh structure, coil, multi-design, or custom design) and their mechanism of expansion (balloon-expandable or self-expanding). Stents must also achieve a variety of characteristics, including thrombo-resistance, corrosion resistance, inflammation resistance, flexibility, radio-opacity, low yield stress, minimal MRI footprint, and radial-strength [40]. Coating stents with blood compatible materials such as gold or various biopolymers has been shown to improve thrombo-resistance in the initial stages of healing [41].

In the previous work [26,30], we identified duplex stainless steel materials known as 2205 stainless steel (2205 SS) as a candidate for magnetic stent design and manufacturing (Fig. 7). This material has similar mechanical and corrosion properties to the 316L stainless steel (used mainly for commercial stents fabrication), but the significant advantage is that it also has weak ferromagnetic properties.

2.3.2. Magnetization of stents

The stents were magnetized using a neodymium rare earth magnet. For stent magnetization, the external magnetic field was generated by two 1.0 T magnets positioned on opposite sides of the stent with opposing poles facing inward during a time interval of 1 min. After the 2205 SS stent magnetization, the retained magnetism was inspected using a Spin TJ magnetometer (Micro Magnetics, Fall River, MA, USA). The investigation was done for eight bent segments and 16 straight segments of the magnetized stent and was compared with a non-magnetized control stent.

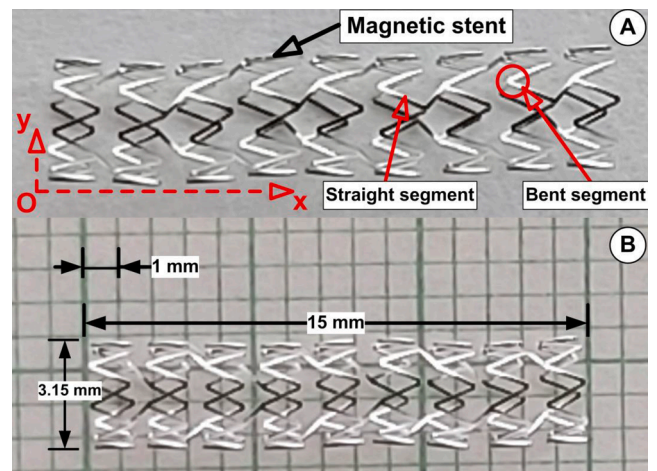


Fig. 7. Ferromagnetic stent. A) General view of the stent geometry. B) The characteristic dimension of the expanded stent. Strut thickness of 0.09 mm.

The stent design was accomplished by using computer-aided design (CAD) (SolidWorks 2009, Dassault Systemes, Providence, RI, USA) and finite element analysis (FEA) (Abaqus 6.9-EF (Dassault Systemes, Providence, RI, USA). Design validation was achieved by fabricating stents and inspecting them for mechanical failure following mechanical crimping and expansion under the medical requirement.

2.3.3. Biological toxicity of the magnetic stent

For biological toxicity, the 2205 SS material was evaluated using tests from the ISO 10,993 standard [30]. The test results have shown that the stent material did not exhibit any biological toxicity effects (report presented in [30], the test performed by Toxicon Corp, Bedford, MA).

2.4. Stented artery model

The real stented artery is variable regarding stent/artery calibers, flow rates, and curvatures. In the real stented geometry, the low wall shear stress (WSS) covers the artery floor around the stent strut vicinity. Our test section is a copy of the realistic post-intervention artery with practical dimensions.

The test sections are fashioned into the right shape from acrylic glass, with a constant internal diameter of 3.15 mm (Fig. 8). Flow experiments were conducted under typical physiological conditions [39]. The mean flow velocity is $U_m = 0.25$ m/s, corresponding to the Reynolds number of $Re = 232$ (based on artery diameter and fluid viscosity).

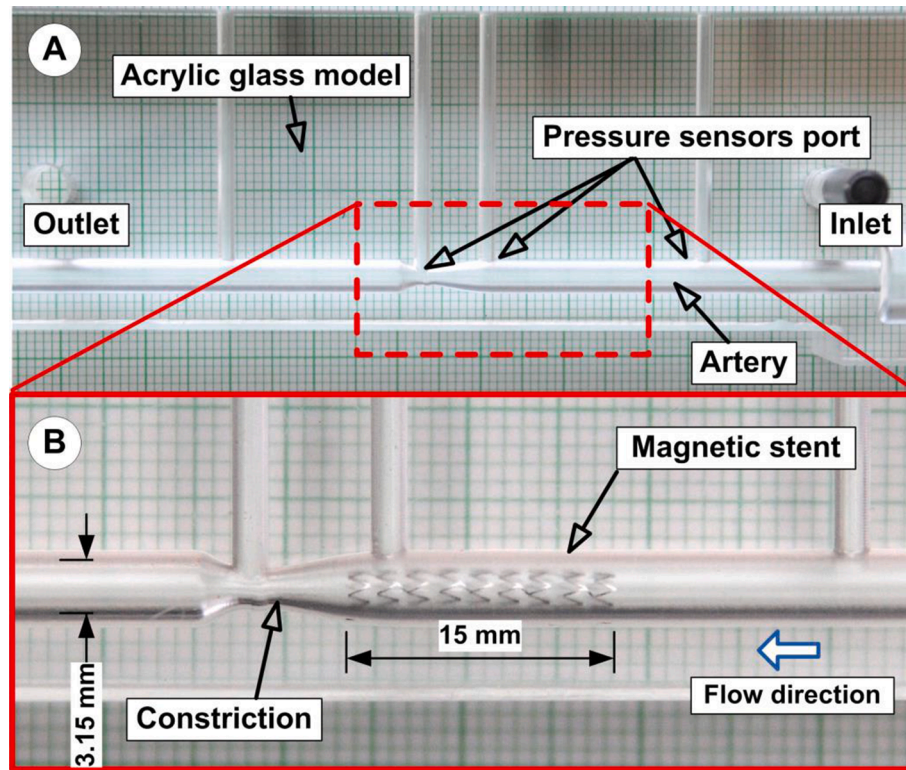


Fig. 8. A) General view of the model artery. B) The magnetically functionalized ferromagnetic stent in the region of investigation.

2.5. Computational fluid dynamics

The purpose of the numerical simulations is to quantify the influence of the luminal flow alterations in the stented artery region and highlight the generation of the recirculation regions around the stent struts.

The computational geometry used for numerical simulations corresponds to the clinically used stent Resolute Integrity Zatarolimus-Eluting Coronary Stent System, Medtronic, USA (geometry detail: internal diameter of 3 mm, length of 15 mm, strut thickness of 0.09 mm), placed inside to the rigid artery model (internal diameter of 3 mm, artery length of 60 mm).

The flow was assumed to be laminar. Blood was modeled as an incompressible fluid, with a particular mass density ρ of the value of 1060 kg/m³. The shear-thinning behavior of blood was accounted for using the non-Newtonian “Carreau” model (presented in section 2.2.1).

The steady simulations’ flow conditions are limited to a single time point within the unsteady cardiac cycle. This time point corresponds to the maximum flow rate during systole and yields a Reynolds number based upon the vessel diameter of $Re = 232$.

The finite volume method (FVM) was adopted to solve the governing equations of fluid motion. The finite-volume computational fluid dynamics code Ansys-Fluent (Ansys 19.2, Ansys Inc., USA) was applied to achieve this aim. The $k-\omega$ turbulent model was used in the present simulation because it can predict low Reynolds number transitional flows inside the stented artery region regions. The inflow boundary conditions were set a flat inflow velocity profile for the axial velocity and zero transverse velocity components at the artery model inlet. The pressure outlet condition was used; namely, the pressure was 0 Pa at the artery exit sections.

3. Magnetic targeting

The magnetic drug targeting involves injection during a specific time. The functionalized single or multi-core magnetic particles delivered in the area of interest by the blood flow under the magnetic force

generated by the externally applied magnetic field. The challenge regarding this technique consists in to create an optimal balance between the hydrodynamic force acting in the human circulatory system and the externally generated magnetic force.

The next sections show our results regarding the efficiency of magnetic drug targeting for the case of the stented coronary artery segment.

3.1. Magnetic field generation

Based in our previous results [26–30], in this paper, a concept of using permanent magnet systems to guide and deliver super-paramagnetic nanoparticles on specific geometry is proposed. The basic idea is to use one external permanent magnet system, which provides a robust enough magnetic field to magnetize, guide, and deliver the MNP’s in the desired region.

For several applications, the magnetic fields are generated using external magnets. The generated magnetic field can vary from ≈ 70 mT to ≤ 1.5 T [42] for in-vitro studies or between 0.1 and 1.5 T [43] for animal trials. In our experiment, the NdFeB50 magnet (or commercial notation N50 – Neodymium 50) permanent magnet from the rare earth family magnet with maximum energy product ($B \times H$) of 50 MGOe was used to generate the magnetic field.

To obtain the magnetic field gradient, we first took measurements of the magnetic flux density within a region of interest perpendicular to the pole face of the test magnet (Fig. 9) using an F.W. Bell Gaussmeter. As can see from Fig. 9B, for the used bar magnet, the magnetic field’s intensity decreases with the distance from the polar piece. However, it can generate magnetic fields ≥ 0.1 T for magnet distance up to 15 mm, and around 0.08 T for magnet distance up to 20 mm, enough to saturate the magnetite. The camcorder monitored the evolution of the MNP’s build-up around the implanted stent in the model artery.

When the distance between the permanent magnet and the stented artery wall is small (less than 15 mm, the gradients of the magnetic field are high (≥ 0.1 T cm⁻¹, Fig. 9B, red dotted line), and the MNP’s can be captured from the flow field in the targeted region and enable stable

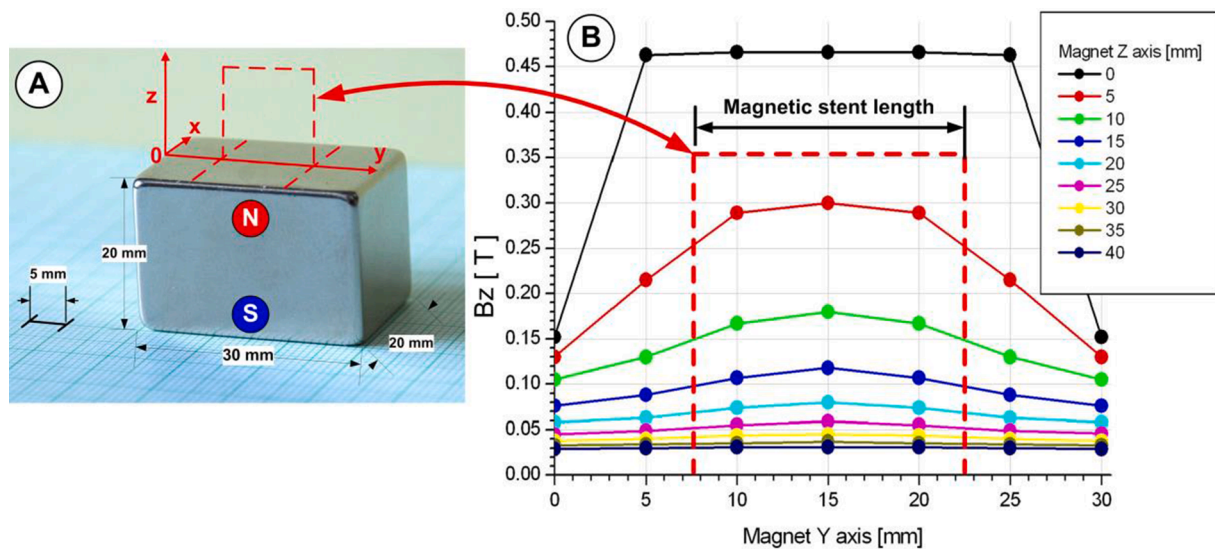


Fig. 9. A magnetic field generated by the NbFeB50 permanent magnet used in the experimental investigation. A). The dimension of the used magnet and axis association. A used permanent magnet has polarization along the Z-axis. B) The figure shown the magnetic field measured with F.W. Bell Gaussmeter, model 5080 in the longitudinal section, along axis Y at the different Z-axis positions.

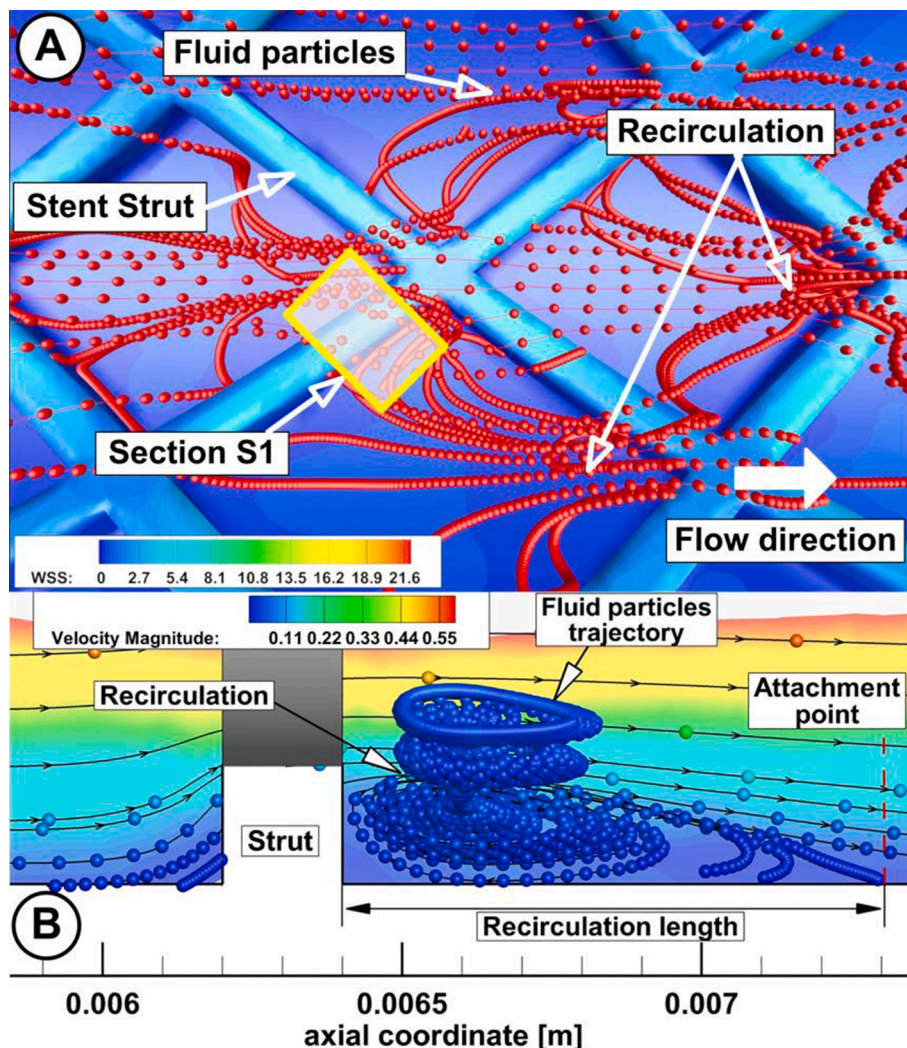


Fig. 10. A) Wall shear stress (WSS) evolution in a stented coronary artery was studied using computational fluid dynamics simulation (Ansys Fluent, Ansys 19.2, Ansys Inc.). The secondary flow caused by the struts' presence is expected to be strongly dependent on the strut geometry characteristics (height and width). This geometric factor will influence the spatial and temporal variations of the velocity field and vicinity of the stent. B) Recirculation zones generated downstream of the strut, characterized by low endothelial shear stress (ESS), increase the local concentration of activated platelets and retard re-endothelialization. Flow patterns around stent struts determine the quantity of the blood-solubilized drug, which is washed away by the free flow stream or trapped in flow stagnation zones and deposited not only under or adjacent to struts but also in distal tissue segments or inter-strut zones. Particle trajectories are in red for Fig A and blue for Fig. B. (For interpretation of the references to colour in this figure legend, the reader is referred to the web version of this article.)

deposit. As expected, if the distance is considerable (small magnetic field gradients are present), the chance of magnetic capture is low, and MNP's, are washed out from the targeted region.

4. Results and discussion

4.1. Flow hydrodynamics

The primary role of blood flow is to transport and dissipate the drug into the targeted vascular region. The primary purpose of this hemodynamics analysis of the blood flow in the stented artery segment was to provide insight into the patterns and the role of flow around stent struts from the targeted drug distribution.

To achieve this goal, a computational numerical simulation was performed of the blood flow around the stent struts and in the inter-strut areas. These numerical simulations were done for the clinically used stent (Resolute Integrity Zatarolimus-Eluting Coronary Stent System, Medtronic, USA). The Resolute Integrity Stent geometry (internal diameter of 3 mm, length of 15 mm, strut thickness of 0.09 mm) have almost the same geometry as our investigated ferromagnetic stent (internal diameter of 3.15 mm, length of 15 mm, strut thickness of 0.09 mm).

These numerical simulations are the first step in the design and optimization of the drug targeting technique to achieve the uniform drug distribution around the implanted stents. In the following paragraphs, we will present the essential aspect of the stent hydrodynamics.

Stent implantation has a significant impact on local flow dynamics since they change native artery geometry and also change the flow condition in the new geometry [44,45]. Stent struts alter normal flow dynamics and create flow separation and recirculation zones around the struts, thereby generate low and high shear stress regions on the artery wall (Fig. 10).

Rigid stent implantation induces acute alterations to the 3-dimensional arterial geometry as results create focal irregularities related to the strut protrusion [11].

The presence of a stent induces changes in arterial geometry and, consequently, in the blood flow and wall shear stress (WSS) patterns. Changing the WSS pattern will change the arterial response to endothelial injury, thereby increasing the risk of in-stent restenosis. Endothelial cells subjected to WSS lower than 0.5 Pa [46], coupled with the flow stagnation region, lead to increased uptake of blood particles to the arterial wall, resulting in increased residence time and increased permeability of the endothelial layer [47]. These vascular deformations modify the flow velocity profiles, reduce the post-implantation WSS along the length of the stent, and alter the focal in-stent WSS distribution. As can see from the figure, the vascular regions between struts generate a recirculation region and, also create a WSS value below of 0.4 Pa. Consequently, this region has shown a strong correlation with

sites of intimal thickening [48].

Low wall shear stress induces the conversion of biomechanical stimuli to biochemical responses by endothelial cells leading to the activation of the inflammatory pathway. However, normal or high endothelial shear stress exerts protective functions by reducing endothelial cell death and proliferation and increasing nitric oxide synthase [49].

For designing an efficient drug targeting system is mandatory to take into account all hemodynamic aspects presented earlier to develop the right magnetic field necessary for a uniform drug particle distribution in the targeted region.

4.2. Particle deposition

In this experiment, the central assumptions were steady laminar flow, constant physical properties of the working fluid and, negligible gravitational effects (Fig. 11B). Capture and deposition of the injected magnetic clusters in the flow stream are based on the competition between the drag force exerted from the moving fluid, and the magnetic force exerted by both the magnetic field gradient generated by the permanent external magnet and the ferromagnetic stent magnetic field (Fig. 11A). The balance between these forces practically dictates the magnetic clusters' guidance and deposition around the ferromagnetic stent (Fig. 12).

Using magnetic field measurements for the used permanent magnet, we estimated that this magnet provided a uniform magnetic field of approximately 0.17 T and 0.07 T at the different locations from the magnet surface (10 mm, respectively 20 mm) (according to Fig. 9). With the ferromagnetic stent placed in the acrylic artery model, the magnetic field remained the same, and it is allowed the generation of magnetic force.

Positioning permanent magnet near to the ferromagnetic stent location has obtained a deviation of the injected coated magnetic clusters within the fluid flux and their capture around the stent struts and, also, onto the downstairs wall of the artery model (Fig. 12).

In this study, depositions of the PEG_CMC were investigated for the following conditions (Table 2):

The model's suspension injection was performed at the constant flow rate (1.5 ml/s), and the exit section of the syringe velocity have the same rate of the working fluid through the artery model. Taking into account that the distance between PEG suspension injection point and the stent is small ($19 \times$ stent diameter ~ 60 mm), practically after the time of 1 s the PEG_CMC start to deposit around the proximal stent struts, and at the stent inlet section (Fig. 12A).

Fig. 12 shows the PEG_CMC accumulation for the different injection time steps, around the stent struts, for the fixed magnet position (magnet position at 15 mm from the stent lower part, and 18.15 mm from the stent upper part, Fig. 11). As can see in Fig. 12 the circulating magnetic

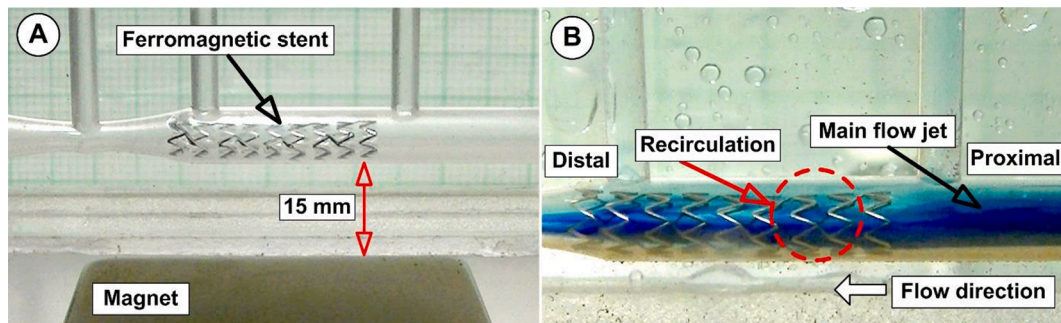


Fig. 11. A) Experimental setup for magnetic particle capturing. B) The flow field in the stented artery model. The presence of the stent induces flow alterations (recirculation) around the stent struts (red circle). The spatial variations of this recirculation are strongly dependent on the strut geometry characteristics (height and width) crown radius (curved section radius), stent cell arrangements (open cells or closed cells), inter-strut angle. (For interpretation of the references to colour in this figure legend, the reader is referred to the web version of this article.)

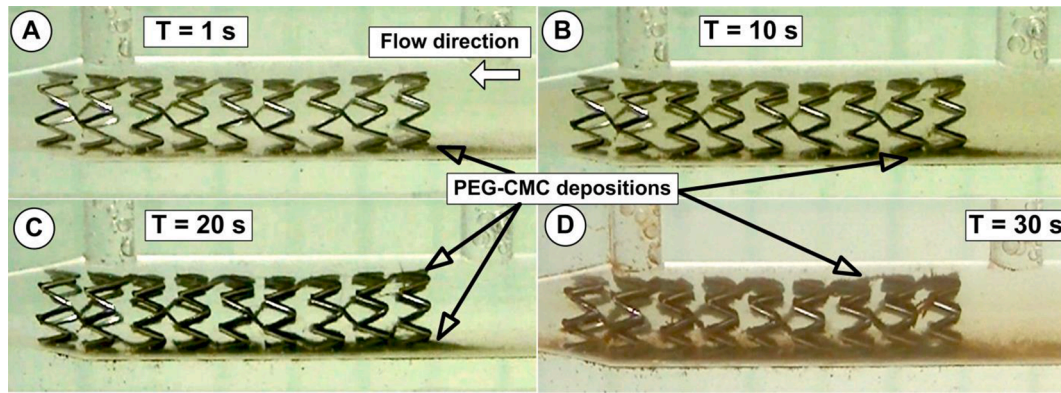


Fig. 12. PEG-CMC deposition in a stented artery segment, and around the stent struts. Magnetic clusters depositions at the different time step of the model suspension injection. A) Time $T = 1$ s, B) $T = 10$ s, C) $T = 20$ s, and D) $T = 30$ s. $T = 0$ s correspond to the start of the injection. The permanent magnet positions were set at the 15 mm from the stent's bottom wall (around 18.15 mm to the top side of the stent), and the corresponding magnetic field intensity B was in the interval of 0.07 T to 0.11 T.

Table 2

Magnetic particles deposition parameters setup.

Parameters	Magnetic cluster diameter (range)	Mean flow velocity	Reynolds number (Re)	Fluid viscosity	Magnetic field induction (at the investigated distance from the stent – interval of 15 mm to 20 mm)
Value	40 ... 150 nm	0.25 m/s	232	0.0036 Pa.s	0.07 T to 0.11 T

clusters progressively cover in time the stent struts. It is essential to observe that the magnetic clusters depositions are uneven, more consistent on the first struts ring (at the stent inlet part), and weaker around the last ring in the stent exit section.

4.3. The role of the ferromagnetic stent in magnetic clusters deposition

In our experiment, the PEG-CMC delivery is achieved by flow-mediated particle transport (Fig. 13). During the injection, from the total amount of injected clusters, a significant quantity was washed out from the stented artery segment. The particle coverage is rather uniformly distributed around the stent struts, with some variability from the stent proximal section to the distal section. This situation happens because local magnetic clusters deposition depends on the stent geometry (struts configuration), and the intensity of the applied external magnetic field. This situation is clearly shown in Fig. 13, where struts from the distal end of the stent were generally not well covered by magnetic clusters, leaving the part of the struts exposed.

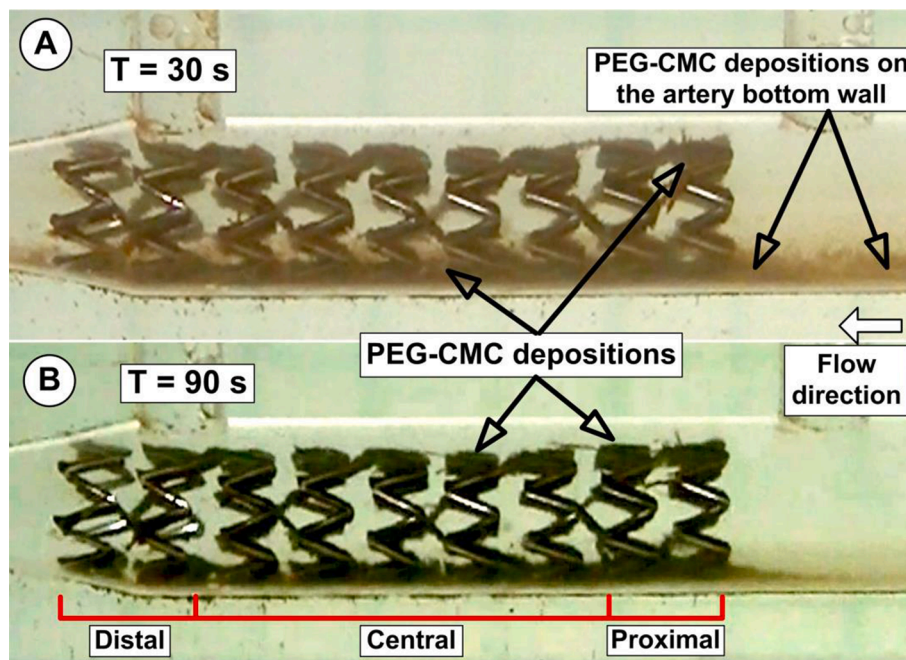


Fig. 13. Comparison of the magnetic cluster deposition in the stented artery at a different moment. A) At the end of the injections period of the 30 s. B) At the 1 min after injections ending. Gross examination of stented coronary relieves the non-uniform strut coverage in different stent segments.

Magnetic clusters deposition occurs when the magnetic force counteracts the flow drag force (Figs. 12 and 13). As a result, the PEG_CMC distributed in the main flow stream is guided to the artery bottom wall where start the accumulation.

It is important to note that the almost uniform strut coverage of the stent segments is due to the competition between the magnetic field of the ferromagnetic stent, and the presence of the recirculation zone around the stent struts (due to the struts orientation transversally to the flow). These aspects confirm that the local hemodynamics play an essential role in cluster deposition around the stent struts.

The presence of the recirculation flow around the struts increased the near-wall residence time and enhanced the magnetic particle deposition. More, the coverage of the struts with magnetic clusters is a result of the balance between the hydrodynamic force generated by the angular velocity of the recirculation region, the magnetic field intensity generated by the ferromagnetic stent and the superimposed external magnetic field.

As can be seen in Fig. 13, due to the magnet's position closer to the lower part of the stent, the accumulation of particles in this area is more pronounced than the accumulation of particles in the upper part of the stent (around the stent elements). Moreover, the magnet position relative to the stent, respectively, the use of a single magnet induces additional particle accumulation on the artery's lower wall.

4.4. Time stability of the strut coverage with PEG_CMC

The particle retention capacity was investigated from two essential aspects for the targeting particle technique, namely, the stability in a time of the particle deposition, respectively, the influence of the model suspension injection time on the struts coverage.

Fig. 13 shows the stability of the particle deposition around the surface of the struts after 1 min of exposure to flow shear stress in the artery model circulation. It is noteworthy the maintenance in time of the particles in the condition of maintaining a constant flow rate in the arterial model, but, in the presence of the external magnetic field. In our opinion, it is due to the stent magnetization. This finding is distinguished from the suspension injection time point of view.

Fig. 14 shows the PEG_CMC depositions after the 30 s (Fig. 14A) and 70 s (Fig. 14B) injection period. It is evident from Fig. 14 that increasing

injection time will increase the struts coverage. Regarding the strut coverage time stability, after 1 min of the stent exposure time to the flow field (maintaining the external magnetic field), the magnetic clusters depositions look undisturbed. Keeping in mind that this investigation does not refer to any magnetic clusters thickness measurements, the presented conclusions are the results of visual interpretations (Fig. 14 red rectangle).

The PEG_CMC deposition for both used injection time was quantified, using an image processing program (ImageJ, <https://imagej.nih.gov/ij/>), measuring the particles' thickness on the artery lower wall (red arrows).

4.5. Correlation with medical practices

In this paper, we did not study the ferromagnetic stent capability to attract alone the magnetic composites without the presence of the concurrent magnetic field generated by the permanent external magnet. To increase this self-coating property probably is necessary to use a stronger ferromagnetic material.

The efficacy of PEG_CMC capture is correlated with the strength of the magnetic force applied to the particles, practically depend on the distance between the used magnet and, also, from the intensity of the generated magnetic field.

In our particular case of the particles targeting of the ferromagnetic stent, the goal to capture the desired quantity of magnetic clusters evenly distributed around all stent struts may be achieved by changing the stent strut pattern (to create a stronger magnetic field), by using a more strongly ferromagnetic material for stent manufacturing and applying a stronger external magnetic field.

In the case of drug delivery by the DES type stent, a quantity of the drugs is lost in the bloodstream; consequently, it does not significantly contribute to healing the diseased arterial wall. Strut positioning within an artery will ultimately be responsible for local fluctuations in arterial drug concentration, both for implanted DES and stent drug targeting. As presented in our previous studies, PEG_CMC can be a useful vehicle to provide sustained local elution and delivery of therapeutic agents.

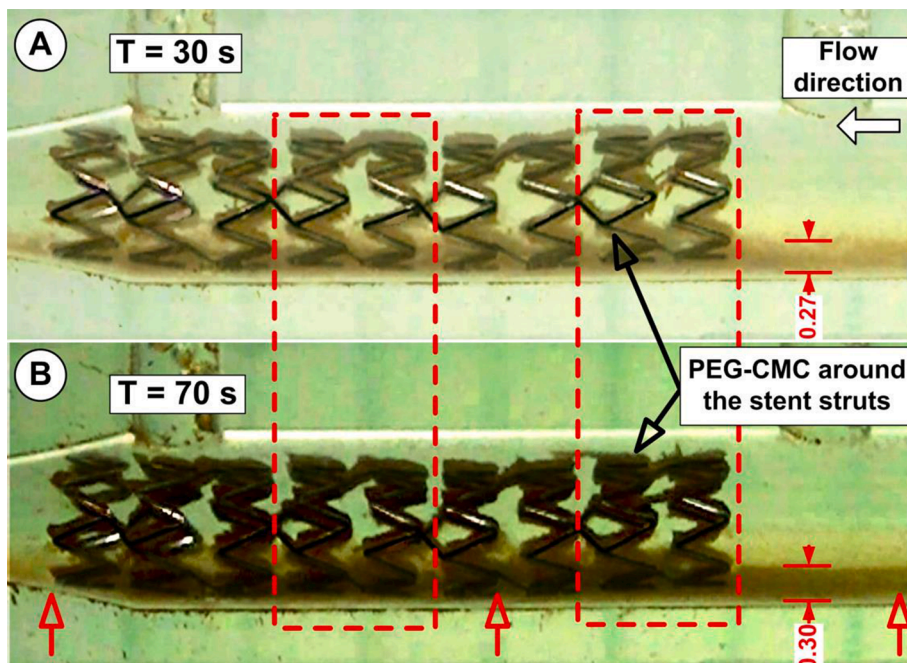


Fig. 14. Comparison of the PEG_CMC deposition in the stented artery for different injection period. A) Injections period of the 30 s. B) Injections period of the 70 s. For both experiments, the same conditions were used, same ferromagnetic stent, the same quantity of the model suspension (20 ml), same flow rate, and the same magnet and magnet position. Gross examination of stent coverage presented in the figures shown that increasing the injection period will increase the particle deposition (red rectangle) around the stent geometry and the sediments in the artery model's lower wall (red arrows). (For interpretation of the references to colour in this figure legend, the reader is referred to the web version of this article.)

5. Clinical perspective

It is proved in clinical practice that after stent placement, struts endothelial coverage was generally complete at the extreme distal and proximal regions of the implanted stent, against the stent middle segments [50]. This irregular endothelial coverage is a result of the flow disturbance due to the stent geometry configurations. More, in the case of drug-eluting stents placement, the arterial wall around the struts is subject to a higher drug exposure than the inter-struts areas exposed to the lower drug concentration [51].

The drugs released during particle targeting are expected to inhibit inflammation and neointimal formation after stent implantation. Detailed understanding of the specific aspects of the magnetically guided drug targeting allows proper selection of the drug carrier used and the magnetic systems used for magnetic field generation.

The drug local targeting strategy presents a good alternative for eliminating the major disadvantage of systemic administration consisting of insufficient therapeutic medication concentrations at the desired site. These localized therapeutics, using drugs targeting through magnetic carriers, are particularly attractive for chronic disease management because this technique can overcome the dose limit toxicity constraint and also can improve drug efficiency [52].

It is essential to mention that targeted drug delivery is not easily controlled. Drug stability, drug release rates, and tissue-specific targeting are challenging to predict.

Commercial stents are typically made from non-magnetic materials (e.g., 304 or 316L stainless steel, cobalt-chromium alloy). The ferromagnetic stent used in this work, due to its duplex austenite/ferrite microstructure [26], exhibits better material characteristics in comparison to the commercial austenitic stainless steel stents (135% higher yield strength, 25% higher ultimate tensile strength, and significant superior corrosion resistance [53]). Also, the expanded ferromagnetic stent does not show any signs of material damage or failure.

Compared with biodurable coating (used for first-generation drug-eluting stents), biodegradable coating like PEG allows a complete release of embedded drug by polymers degradation. Consequently, it is an adequate candidate for the local drug targeting technique [54].

Due to the PEG low toxicity, this polymer is used for various applications like dispersant or skin creams. More, the results of biocompatibility analysis demonstrated that PEGylated MNP's have excellent potential for clinical applications.

6. Next steps

Related to improving the stent's magnetic performance, we want to investigate the influence of changing stent geometry (position of structures and connectors) on the stent's magnetic field and the possibility of using an external magnetic configuration to generate more uniform magnetization on stent elements.

Regarding the quantitative evaluation of the PEG_CMC clusters depositions and also the amount of eluted clusters, in the next step, we intend to use a more simplified stented artery geometry to facilitate a precise measurement (mass measurements, spectrophotometer, or UV detector) of the all involved model elements.

We intend to use different external magnet configurations regarding magnets, positions, dimensions, and types to generate more uniform stent coverage with clusters.

Also, to avoid incomplete endothelialization between the stent struts and, in the strut vicinity, we intend to investigate the effects of the stent malapposition (lack of contact between at least one stent strut and the arterial wall) on the magnetic targeting efficiency.

7. Conclusions

The goal of this paper is to highlight the advantages and feasibility of the site's specific targeting of the PEG_CMC, in the particular cases of the

arterial stent placement.

We focus on proving the feasibility of the proposed delivery systems during this work to provide a sustained and controlled local particle delivery to reduce the adverse side effects to the tissue surrounding the implanted stent.

In the present paper, we have developed a strategy to use the magnetic forces to guide and capture PEG_CMC to the implanted stent device's surface. The use of the artery mimics in these experimental setup means assuring the physiological drug transport mechanisms and the adequate capture effects of magnetic clusters in specific sites. Our basic concepts are that the magnetic clusters flow freely in the vascular system and can be easily guided using an external magnetic field to the desired artery segment.

For the development of the flow system, results from the medical literature were taken into account, which suggests that to improve the efficiencies of injected drugs for local therapy, the artery administration of drugs is more effective than intravenous administration, because the medication could be transported directly and much faster to the desired locations [55].

For stent surface targeting, we used PEG coated magnetic nano-clusters. To design this work, we took into account all of the advantages of the PEG-coated MNP's namely engineered cluster size between 40 and 150 nm (provide enhanced delivery capability), stability, improved bioavailability, high loading capacity, low toxicity, and prolonged retention time.

In our previous studies, *in vitro* investigations have been conducted to analyze cytotoxicity for ferromagnetic stent and, also the PEG_CMC. Previous cytotoxicity analyses demonstrated that the investigated devices have excellent biocompatibility and promising potential in clinical applications.

Declaration of Competing Interest

The authors declare that they have no known competing financial interests or personal relationships that could have appeared to influence the work reported in this paper.

Acknowledgments

For S.I. Bernad, this work was partially supported by the RA-TB/CFATR/LHC multiannual research program 2016–2020, and partly by a mobility grant of the Romanian Ministry of Research and Innovation, CNCS-UEFISCDI, project number PN-III-P1-1.1-MC-2019-0630. For L. Vekas the work was supported by the RA-TB/CFATR/LMF multiannual research program 2016–2020 and by a grant of the Romanian Ministry of Research and Innovation, CCCDIUEFISCDI, project number PN-III-PI-1,2-PCCDI-2017-0871, contract c47PCCDI/2018. For I. Craciunescu and R. Turcu this work was supported by the subsidiary contract for industrial research and experimental development nr. 270/2018. The authors are grateful to Daniela Susan-Resiga (Romanian Academy – Timisoara Branch) for rheological measurements.

References

- [1] J.J. Wentzel, D.M. Whelan, W.J. van der Giessen, H.M.M. van Beusekom, I. Andhyiswara, P.W. Serruys, C.J. Slager, R. Krams, Coronary stent implantation changes 3-D vessel geometry and 3-D shear stress distribution, *J. Biomech.* 33 (10) (2000) 1287–1295, [https://doi.org/10.1016/S0021-9290\(00\)00066-X](https://doi.org/10.1016/S0021-9290(00)00066-X).
- [2] J.J. Wentzel, F.J.H. Gijzen, J.C.H. Schuurbers, A.F.W. van der Steen, P.W. Serruys, The influence of shear stress on in-stent restenosis and thrombosis, *EuroIntervention.* 4 (Supl.C) (2008) C27–C32.
- [3] H.Y. Chen, J. Hermiller, A.K. Sinha, M. Sturek, L. Zhu, G.S. Kassab, Effects of stent sizing on endothelial and vessel wall stress: potential mechanisms for in-stent restenosis, *J. Appl. Physiol.* 106 (2009) 1686–1691.
- [4] S.-J. Park, S.-J. Kang, R. Virmani, M. Nakano, Y. Ueda, In-stent neoatherosclerosis: a final common pathway of late stent failure, *J. Am. Coll. Cardiol.* 59 (2012) 2051–2057.
- [5] R. Ross, Atherosclerosis: an inflammatory disease, *N. Engl. J. Med.* 340 (1999) 115–126.

- [6] A.V. Finn, G. Nakazawa, M. Joner, F.D. Kolodgie, E.K. Mont, H.K. Gold, R. Virmani, Vascular responses to drug eluting stents: importance of delayed healing, *ATVB* 27 (7) (2007) 1500–1510, <https://doi.org/10.1161/ATVBAHA.107.144220>.
- [7] M. Joner, A.V. Finn, A. Farb, E.K. Mont, F.D. Kolodgie, E. Ladich, R. Kutys, K. Skorija, H.K. Gold, R. Virmani, Pathology of drug-eluting stents in humans: delayed healing and late thrombotic risk, *J. Am. Coll. Cardiol.* 48 (1) (2006) 193–202.
- [8] M. Gilard, P. Barragan, A.A.L. Noryani, H.A. Noor, T. Majwal, T. Hovasse, P. Castellant, M. Schneeberger, L. Maillard, E. Bressolette, J. Wojcik, N. Delarche, D. Blanchard, B. Jouve, O. Ormezzano, F. Paganelli, G. Levy, J. Sainsous, D. Carrie, A. Furber, J. Berland, O. Darremont, H. Le Breton, A. Lyuyx-Bore, A. Gommeaux, C. Cassat, A. Kermarrec, P. Cazaux, P. Druelles, R. Dauphin, J. Armengaud, P. Dupouy, D. Champagnac, P. Ohlmann, K. Endresen, H. Benamer, R.G. Kiss, I. Ungi, J. Bosch, M.-C. Morice, 6-versus 24-month dual antiplatelet therapy after implantation of drug-eluting stents in patients nonresistant to aspirin, *J. Am. Coll. Cardiol.* 65 (8) (2015) 777–786, <https://doi.org/10.1016/j.jacc.2014.11.008>.
- [9] A. Colombo, A. Chieffo, A. Frasieri, R. Garbo, M. Masotti-Centol, N. Salvatella, J. F. Oteo Dominguez, L. Steffanon, G. Tarantini, et al., Second-generation drug-eluting stent implantation followed by 6- versus 12-month dual antiplatelet therapy: the SECURITY randomized clinical trial, *J. Am. Coll. Cardiol.* 64 (2014) 2086.
- [10] L. Mauri, D.J. Kereiakes, R.W. Yeh, P. Driscoll-Shempp, D.E. Cutlip, P.G. Steg, S. L. Normand, E. Braunwald, S.D. Wiviott, D.J. Cohen, D.R. Jr Holmes, et al., Twelve or 30 months of dual antiplatelet therapy after drug-eluting stents, *N. Engl. J. Med.* 371 (2014) 2155.
- [11] Yongzhi Qiu, Sheng Tong, Linlin Zhang, Yumiko Sakurai, David R. Myers, Lin Hong, Wilbur A. Lam, Gang Bao, Magnetic forces enable controlled drug delivery by disrupting endothelial cell-cell junctions, *Nat. Commun.* 8 (1) (2017), <https://doi.org/10.1038/ncomms15594>.
- [12] L. Lartigue, P. Hugouneq, D. Alloeyau, S.P. Clarke, M. Levy, J.-C. Bacri, R. Bazzi, D. F. Brougham, C. Wilhelm, F. Gazeau, Cooperative organization in iron oxide multi-core nanoparticles potentiates their efficiency as heating mediators and MRI contrast agents, *ACS Nano* 6 (12) (2012) 10935–10949, <https://doi.org/10.1021/nn304477s>.
- [13] E. Tombácz, R. Turcu, V. Socoliuc, L. Vékás, Magnetic iron oxide nanoparticles: Recent trends in design and synthesis of magnetoresponsive nanosystems, *Biochem. Biophys. Res. Commun.* 468 (3) (2015) 442–453, <https://doi.org/10.1016/j.bbrc.2015.08.030>.
- [14] Minghan Hu, Hans-Jürgen Butt, Katharina Landfester, Markus B. Bannwarth, Sanghyuk Woo, Héloïse Thérien-Aubin, Shaping the assembly of superparamagnetic nanoparticles, *ACS Nano* 13 (3) (2019) 3015–3022, <https://doi.org/10.1021/acsnano.8b07783.s007>.
- [15] S. Dürr, C. Janko, S. Lye, P. Tripal, M. Schwarz, Z. Jan, R. Tietze, C. Alexiou, Magnetic nanoparticles for cancer therapy, *Nanotechnol. Rev.* 2 (2013) 395–409.
- [16] S. Laurent, A.A. Saei, S. Behzadi, A. Panahif, M. Mahmoudi, Super-paramagnetic iron oxide nanoparticles for delivery of therapeutic agents: opportunities and challenges, *Expert Opin. Drug. Deliv.* 11 (2014) 1–22.
- [17] S.K. Suh, K. Yuet, D.K. Hwang, K.W. Bong, S.S. Doyle, T.A. Hatton, Synthesis of non-spherical super-paramagnetic particles: In situ coprecipitation of magnetic nanoparticles in microgels prepared by stop-flow lithography, *J. Am. Chem. Soc.* 134 (2012) 7337–7343.
- [18] Miriam Colombo, Susana Carregal-Romero, María F. Casula, Lucía Gutiérrez, María P. Morales, Ingrid B. Böhm, Johannes T. Heverhagen, Davide Prosperi, Wolfgang J. Parak, Biological applications of magnetic nanoparticles, *Chem. Soc. Rev.* 41 (11) (2012) 4306, <https://doi.org/10.1039/c2cs15337h>.
- [19] Boru Zhu, Thomas Eurrell, Rico Gunawan, Deborah Leckband, Chain-length dependence of the protein and cell resistance of oligo(ethylene glycol)-terminated self-assembled monolayers on gold, *J. Biomed. Mater. Res.* 56 (3) (2001) 406–416, [https://doi.org/10.1002/1097-4636\(20010905\)56:3<406::AID-JBM1110>3.0.CO;2-R](https://doi.org/10.1002/1097-4636(20010905)56:3<406::AID-JBM1110>3.0.CO;2-R).
- [20] A.E. Nel, L. Mädler, D. Velegol, T. Xia, E.M.V. Hoek, P. Somasundaran, F. Klaessig, V. Castranova, M. Thompson, Understanding biophysicochemical interactions at the nano-bio interface, *Nat. Mater.* 8 (2009) 543–557.
- [21] Amir Ata Saei, Mahdieh Yazdani, Samuel E. Lohse, Zahra Bakhtiary, Vahid Serpooshan, Mahdi Ghavami, Mahtab Asadian, Samaneh Mashaghi, Erik C. Dreaden, Alireza Mashaghi, Morteza Mahmoudi, Nanoparticle surface functionality dictates cellular and systemic toxicity, *Chem. Mater.* 29 (16) (2017) 6578–6595, <https://doi.org/10.1021/acs.chemmater.7b01979>.
- [22] E. Illés, M. Szekeres, I.Y. Tóth, K. Farkas, I. Földesi, Á. Szabó, B. Iván, E. Tombácz, PEGylation of Superparamagnetic Iron Oxide Nanoparticles with Self-Organizing Polyacrylate-PEG Brushes for Contrast Enhancement in MRI Diagnosis, *Nanomaterials* 8 (2018) 776, <https://doi.org/10.3390/nano8100776>.
- [23] Erzsébet Illés, Márta Szekeres, Edina Kupcsik, Ildikó Y. Tóth, Katalin Farkas, Angéla Jedlovsky-Hajdú, Eteleka Tombácz, PEGylation of surfactant magnetite core-shell nanoparticles for biomedical application, *Colloids Surf., A* 460 (2014) 429–440, <https://doi.org/10.1016/j.colsurfa.2014.01.043>.
- [24] Ildikó Y. Tóth, Erzsébet Illés, Rita A. Bauer, Dániel Nesztör, Márta Szekeres, István Zupkó, Eteleka Tombácz, Designed polyelectrolyte shell on magnetite nanocore for dilution-resistant biocompatible magnetic fluids, *Langmuir* 28 (48) (2012) 16638–16646, <https://doi.org/10.1021/ja302660p>.
- [25] Angéla Hajdú, Márta Szekeres, Ildikó Y. Tóth, Rita A. Bauer, Judith Mihály, István Zupkó, Eteleka Tombácz, Enhanced stability of polyacrylate-coated magnetite nanoparticles in biorelevant media, *Colloids Surf., B* 94 (2012) 242–249, <https://doi.org/10.1016/j.colsurfb.2012.01.042>.
- [26] S. Uthamaraj, B.J. Tefft, M. Klabusay, O. Hlinomaz, G.S. Sandhu, D. Dragomir-Daescu, Design and validation of a novel ferromagnetic bare metal stent capable of capturing and retaining endothelial cells, *ABME* 42 (2014) 2416.
- [27] S.V. Pislaru, A. Harbuzariu, R. Gulati, T. Witt, N.P. Sandhu, R.D. Simari, G. S. Sandhu, Magnetically targeted endothelial cell localization in stented vessels, *J. Am. Coll. Cardiol.* 48 (2006) 1839.
- [28] Henrik Kempe, Steven A Kates, Maria Kempe, Nanomedicine's promising therapy: magnetic drug targeting, *Expert Rev. Med. Devices* 8 (3) (2011) 291–294, <https://doi.org/10.1586/erd.10.94>.
- [29] S. Uthamaraj, B.J. Tefft, O. Hlinomaz, G.S. Sandhu, D. Dragomir-Daescu, Ferromagnetic bare metal stent for endothelial cell capture and retention, *JOVE* 103 (2015), e53100.
- [30] B.J. Tefft, S. Uthamaraj, A. Harbuzariu, J.J. Harburn, T.A. Witt, B. Newman, P. J. Psaltis, O. Hlinomaz, D.R. Holmes Jr, R. Gulati, R.D. Simari, D. Dragomir-Daescu, G.S. Sandhu, Nanoparticle-mediated cell capture enables rapid endothelialization of a novel bare metal stent, *Tissue Eng. Part A* 24 (13–14) (2018) 1157–1166, <http://doi:10.1089/ten.TEA.2017.0404>.
- [31] S.I. Bernad, D. Susan-Resiga, E. Bernad, Hemodynamic effects on particle targeting in the arterial bifurcation for different magnet positions, *Molecules* 24 (13) (2019) 2509, <https://doi.org/10.3390/molecules24132509>.
- [32] S.I. Bernad, D. Susan-Resiga, L. Vekas, E.S. Bernad, Drug targeting investigation in the critical region of the arterial bypass graft, *J. Magn. Magn. Mater.* 475 (2019) 14–23.
- [33] D. Bica, Preparation of magnetic fluids for various applications, *Rom Repts Phys.* 47 (3–5) (1995) 265–272.
- [34] R. Turcu, V. Socoliuc, I. Craciunescu, A. Petran, A. Paulus, M. Franzreb, E. Vasile, L. Vekas, Magnetic microgels, a promising candidate for enhanced magnetic adsorbent particles in bioseparation: synthesis, physicochemical characterization, and separation performance, *Soft Matter* 11 (2015) 1008–1018, <https://doi.org/10.1039/C4SM02430C>.
- [35] Y.I. Cho, K.R. Kensey, Effects of the non-Newtonian viscosity of blood on flows in a diseased arterial vessel. Part 1: Steady flows, *Biorheology* 28 (3–4) (1991) 241–262.
- [36] D. Susan-Resiga, D. Bica, L. Vekas, Flow behavior of extremely bidisperse magnetizable fluids, *J. Magn. Magn. Mater.* 322 (20) (2010) 3166–3172.
- [37] T.G. Mezger, *The Rheology Handbook*, Curt R. Vincent Verlag, Hannover, 2002.
- [38] Habib Samady, Parham Eshtehardi, Michael C. McDaniel, Jin Suo, Saurabh S. Dhawan, Charles Maynard, Lucas H. Timmins, Arshed A. Quyyumi, Don P. Giddens, Coronary artery wall shear stress is associated with progression and transformation of atherosclerotic plaque and arterial remodeling in patients with coronary artery disease, *Circulation* 124 (7) (2011) 779–788, <https://doi.org/10.1161/CIRCULATIONAHA.111.021824>.
- [39] R. Torii, N.B. Wood, N. Hadjiloizou, A.W. Dowsey, A.R. Wright, A.D. Hughes, J. Davies, D.P. Francis, J. Mayet, G. Yang, S.A. Thom, X.Y. Xu, Stress phase angle depicts differences in coronary artery hemodynamics due to changes in flow and geometry after percutaneous coronary intervention, *Am. J. Physiol.-Heart Circulatory Physiol.* 296 (3) (2009) H765–H776, <https://doi.org/10.1152/ajpheart.01166.2007>.
- [40] C. Lally, F. Dolan, P.J. Prendergast, Cardiovascular stent design and vessel stresses: a finite element analysis, *J. Biomech.* 38 (8) (2005) 1574–1581, <https://doi.org/10.1016/j.jbiomech.2004.07.022>.
- [41] Elazer R. Edelman, Philip Seifert, Adam Groothuis, Alisa Morss, Danielle Bornstein, Campbell Rogers, Gold-coated NIR stents in porcine coronary arteries, *Circulation* 103 (3) (2001) 429–434, <https://doi.org/10.1161/01.CIR.103.3.429>.
- [42] R. Jurgons, C. Seliger, A. Hilpert, L. Trahms, S. Odenbach, C. Alexiou, Drug loaded magnetic nanoparticles for cancer therapy, *J. Phys.: Condens. Matter* 18 (38) (2006) S2893–S2902, <https://doi.org/10.1088/0953-8984/18/38/S24>.
- [43] Katja Schulze, Annette Koch, Bernhard Schöpf, Alke Petri, Benedikt Steitz, Mathieu Chastellain, Margarethe Hofmann, Heinrich Hofmann, Brigitte von Rechenberg, Intraarticular application of superparamagnetic nanoparticles and their uptake by synovial membrane—an experimental study in sheep, *J. Magn. Magn. Mater.* 293 (1) (2005) 419–432, <https://doi.org/10.1016/j.jmmm.2005.02.075>.
- [44] E.S. Bernad, C.I. Hudrea, S.I. Bernad, A. F. Totorean, A. I. Bosioc, Luminal flow alteration in presence of the stent, International Conference of Computational Methods in Sciences and Engineering 2015 (ICCMSE 2015), AIP Conf. Proc. 1702 (2015) 080011-1-080011-4, <https://doi.org/10.1063/1.4938806>.
- [45] A.F. Totorean, C.I. Hudrea, A.I. Bosioc, S.I. Bernad, Flow field evolution in stented versus stenosed coronary artery, *Proc. Rom. Acad. Ser. A-Math. Phys.* 18 (3) (2017) 248–255.
- [46] J.K. Jiménez, P.F. Davies, Hemodynamically Driven Stent Strut Design, *Ann. Biomed. Eng.* 37 (8) (2009) 1483, <https://doi.org/10.1007/s10439-009-9719-9>.
- [47] J.B. Murphy, F.J. Boyle, Predicting neointimal hyperplasia in stented arteries using time-dependent computational fluid dynamics: a review, *Comput. Biol. Med.* 40 (2010) 408–418.
- [48] Juan Mejia, Bilal Ruzzeah, Rosaire Mongrain, Richard Leask, Olivier F Bertrand, Evaluation of the effect of stent strut profile on shear stress distribution using statistical moments, *Biomed. Eng. Online* 8 (1) (2009) 8, <https://doi.org/10.1186/1475-925X-8-8>.
- [49] N.E. Hastings, M.B. Simmers, O.G. McDonald, B.R. Wamhoff, B.R. Blackman, Atherosclerosis-prone hemodynamics differentially regulate endothelial and smooth muscle cell phenotypes and promotes pro-inflammatory priming, *Am. J. Physiol. Cell Physiol.* 293 (2007) C1824–C1833.
- [50] Yoram Richter, Elazer R. Edelman, Cardiology is flow, *Circulation* 113 (23) (2006) 2679–2682, <https://doi.org/10.1161/CIRCULATIONAHA.106.632687>.

- [51] C.D.K. Rogers, Drug-eluting stents: role of stent design, delivery vehicle, and drug selection, *Rev Cardiovasc Med.* 3 (2002) S10–S15.
- [52] Mark W. Tibbitt, James E. Dahlman, Robert Langer, Emerging frontiers in drug delivery, *J. Am. Chem. Soc.* 138 (3) (2016) 704–717, <https://doi.org/10.1021/jacs.5b09974>.
- [53] Wen-Ta Tsai, Ming-Shan Chen, Stress corrosion cracking behavior of 2205 duplex stainless steel in concentrated NaCl solution, *Corros. Sci.* 42 (3) (2000) 545–559, [https://doi.org/10.1016/S0010-938X\(99\)00105-5](https://doi.org/10.1016/S0010-938X(99)00105-5).
- [54] Teruo Inoue, Kevin Croce, Toshifumi Morooka, Masashi Sakuma, Koichi Node, Daniel I. Simon, Vascular inflammation and repair, *JACC: Cardiovascular Interventions* 4 (10) (2011) 1057–1066, <https://doi.org/10.1016/j.jcin.2011.05.025>.
- [55] Kohei Tahara, Yuta Miyazaki, Yoshiaki Kawashima, Jörg Kreuter, Hiromitsu Yamamoto, Brain targeting with surface-modified poly(D,L-lactic-co-glycolic acid) nanoparticles delivered via carotid artery administration, *Eur. J. Pharm. Biopharm.* 77 (1) (2011) 84–88, <https://doi.org/10.1016/j.ejpb.2010.11.002>.